THE GERONTOLOGICAL SOCIETY OF AMERICA®

Journals of Gerontology: Biological Sciences
cite as: *J Gerontol A Biol Sci Med Sci*, 2017, Vol. 72, No. 3, 329–337
doi:10.1093/gerona/glw088
Advance Access publication May 21, 2016

OXFORD

Original Article

Enhanced Cognition and Hypoglutamatergic Signaling in a Growth Hormone Receptor Knockout Mouse Model of Successful Aging

Kevin N. Hascup,[1] Mary K. Lynn,[2] Patrick J. Fitzgerald,[1] Shari Randall,[1] John J. Kopchick,[3] Heather A. Boger,[2,4] Andrzej Bartke,[5] and Erin R. Hascup[1,6]

[1]Department of Neurology, Center for Alzheimer's Disease and Related Disorders, Southern Illinois University School of Medicine, Springfield. [2]Department of Neuroscience, Medical University of South Carolina, Charleston. [3]Edison Biotechnology Institute, Department of Biomedical Sciences, Ohio University, Athens. [4]Center on Aging, Medical University of South Carolina, Charleston. [5]Department of Internal Medicine and [6]Department of Pharmacology, Southern Illinois University School of Medicine, Springfield.

Address correspondence to Erin R. Hascup, PhD, Department of Neurology, Center for Alzheimer's Disease and Related Disorders, Southern Illinois University School of Medicine, PO Box 19628, Springfield, IL 62794-9628. E-mail: ehascup@siumed.edu

Received November 2, 2015; Accepted April 25, 2016

Decision Editor: Rafael de Cabo, PhD

Abstract

Growth hormone receptor knockout (GHR-KO) mice are long lived with improved health span, making this an excellent model system for understanding biochemical mechanisms important to cognitive reserve. The purpose of the present study was to elucidate differences in cognition and glutamatergic dynamics between aged (20- to 24-month-old) GHR-KO and littermate controls. Glutamate plays a critical role in hippocampal learning and memory and is implicated in several neurodegenerative disorders, including Alzheimer's disease. Spatial learning and memory were assessed using the Morris water maze (MWM), whereas independent dentate gyrus (DG), CA3, and CA1 basal glutamate, release, and uptake measurements were conducted in isoflurane anesthetized mice utilizing an enzyme-based microelectrode array (MEA) coupled with constant potential amperometry. These MEAs have high temporal and low spatial resolution while causing minimal damage to the surrounding parenchyma. Littermate controls performed worse on the memory portion of the MWM behavioral task and had elevated DG, CA3, and CA1 basal glutamate and stimulus-evoked release compared with age-matched GHR-KO mice. CA3 basal glutamate negatively correlated with MWM performance. These results support glutamatergic regulation in learning and memory and may have implications for therapeutic targets to delay the onset of, or reduce cognitive decline, in Alzheimer's disease.

Keywords: Alzheimer's disease—Biosensor—Electrode—Health span—Longevity

Growth hormone (GH) is secreted by the anterior pituitary gland and binds to its receptor ubiquitously expressed throughout the mammalian reproductive, muscular, endocrine, and nervous systems, where it regulates growth and metabolism often mediated through insulin-like growth factor-I (IGF-1) (1). The GH/IGF-1 axis is regarded as an important regulator in aging such that attenuated signaling increases life span (2), potentially by providing protection against cancer, diabetes, and neurodegeneration (3). This is supported by GH receptor knockout (GHR-KO) mice that exhibit increased life span (30–36 months) and improved health span (reduced and delayed incidence of neoplasty, protection from diet-induced nephropathy, and retained cognitive abilities). Furthermore, inhibition of GH has been shown to increase neuronal differentiation (4), and GHR-KO mice have an approximate 25% increase in total neuron cell density in the cortex (5). However, these benefits come at a concession of decreased size with increased adiposity, similar to Laron Syndrome (6–10).

The increased life span of GHR-KO mice makes them an excellent model system for studying age-related cognitive reserve and neurotransmitter regulation in comparison with littermate controls. For example, recent data support that GHR-KO mice maintain hippocampal glutamatergic function from 4–22 months of age, including vesicular glutamate transporter (VGLUT) 1 (the predominant

hippocampal VGLUT located in classical excitatory terminals (11)) and 3, glutamate transporter 1 (GLT-1), and the N-methyl-d-aspartate (NMDA) receptor subtype GluN2B (12). Glutamate, the predominant excitatory neurotransmitter in the mammalian central nervous system, has a strong prevalence in neocortical and hippocampal pyramidal neurons; therefore, playing a critical role in learning and memory (13). Because of this, glutamate dysregulation has been implicated in age-related cognitive decline associated with neurodegenerative disorders such as Alzheimer's disease (13–17).

The purpose of the present study was to elucidate differences in cognition and glutamatergic dynamics between aged (20- to 24-month-old) GHR-KO and age-matched littermate controls. Spatial learning and memory were assessed using the Morris water maze (MWM) behavioral paradigm (18–20). Extracellular glutamate dynamics were studied in the dorsal hippocampus, because this region is important for consolidation and retrieval of spatial memory (21). Glutamate measurements were conducted utilizing an enzyme-based microelectrode array (MEA) coupled with constant potential amperometry to independently measure basal glutamate and stimulus-evoked glutamate release, and uptake in the dentate gyrus (DG), CA3, and CA1 of isoflurane anesthetized littermate controls and GHR-KO mice. These MEAs have high temporal (4 Hz) (22) and low spatial resolution (50 × 100 µm) while causing minimal damage to the surrounding parenchyma (50–100 µm) (23). The results presented here support the importance of glutamatergic regulation for learning and memory in the GHR-KO mouse model of successful aging.

Methods

Animals

Female GHR-KO (20–24 months of age) and age-matched female normal littermate controls were produced in a breeding colony maintained at Southern Illinois University School of Medicine. This colony was established by crossing 129Ola/BALB/c GHR +/– breeders (24) provided by J.J.K. with mice derived from crosses of C57BL/6J and C3H/J strains and maintained as a closed colony with inbreeding minimized by avoiding brother × sister matings (25). Protocols for animal use were approved by the Laboratory Animal Care and Use Committee at Southern Illinois University School of Medicine. Animals were group housed on a 12:12 hour light: dark cycle, and food and water were available ad libitum. Each mouse underwent cognitive assessment, in vivo glutamate recordings, and postmortem histological analysis of brain tissue with the exception of a loss of two GHR-KO mice that occurred after MWM due to complications during surgery prior to in vivo electrochemistry. Immediately following in vivo glutamate recordings, mice were euthanized with an overdose of isoflurane and decapitated. Upon decapitation, 5-mm tail snips were collected and stored at −80°C until shipment to Transnetyx (Cordova, TN) for genotype verification.

Chemicals

All chemicals were prepared and stored according to manufacturer recommendations unless otherwise noted. l-glutamate oxidase (EC 1.4.3.11) was obtained from Cosmo Bio (Carlsbad, CA) and diluted in distilled, deionized water to make a 1 U/µL stock solution that was stored at 4°C. Sodium phosphate monobasic monohydrate, sodium phosphate dibasic anhydrous, 1,3-phenylenediamine dihydrochloride (mPD), sodium chloride, calcium chloride dehydrate, and hydrogen peroxide (H_2O_2, 30% in water) were obtained from Thermo Fisher Scientific (Waltham, MA). l-glutamic acid sodium salt, potassium chloride, bovine serum albumin (BSA), glutaraldehyde, dopamine hydrochloride (DA), l-ascorbic acid (AA), and dibutyl phthalate and xylene (DPX) were obtained from Sigma-Aldrich (St. Louis, MO). Rabbit polyclonal glial fibrillary acidic protein (GFAP) antibody was obtained from Dako (Carpinteria, CA). Guinea pig polyclonal VGLUT1 antibody was obtained from Millipore (Temecula, CA). Biotinylated goat anti-rabbit serum, biotinylated goat anti-guinea pig serum, avidin-biotin complex (ABC) kit, and VIP peroxidase substrate kit were obtained from Vector Laboratories (Burlingame, CA).

Morris Water Maze

The MWM tests spatial learning and memory by requiring the mouse to utilize visual clues for locating a static, submerged platform, regardless of the starting quadrant as previously reported (20). The MWM paradigm consists of five consecutive learning days with three, 90-second trials per day and a minimum of 20 minutes between trials. After 2 days without testing, mice are given a single, 60-second probe challenge to test memory. The ANY-maze video tracking system (Stoelting, Wood Dale, IL) records and analyzes duration in each quadrant, distance traveled, average speed, and path efficiency for the five learning days. Additional parameters analyzed for the single probe trial include the number of platform crosses, time in annulus 40, latency, distance, and path efficiency to first platform cross.

In Vivo Glutamate Measurements

Enzyme-based MEAs

Enzyme-based MEAs with platinum (Pt) recording surfaces (Figure 1A and B) were fabricated, assembled, coated, and calibrated for in vivo mouse glutamate measurements (22,26,27). Briefly, one of the R2 MEA Pt sites was coated with l-glutamate oxidase, BSA, and glutaraldehyde coating solution. BSA and glutaraldehyde increase the adhesion and crosslink l-glutamate oxidase to the MEA surface. l-glutamate oxidase causes the enzymatic breakdown of glutamate to α-ketoglutarate and the electroactive reporter molecule, H_2O_2. The second Pt recording site (self-referencing or sentinel site) was coated similar to the glutamate recording site, except l-glutamate oxidase was omitted from the coating solution; therefore, the sentinel site was unable to enzymatically generate H_2O_2 from l-glutamate. A potential of +0.7 V versus a Ag/AgCl reference electrode was applied to the Pt recording surface, resulting in a two-electron oxidation of H_2O_2, and the current was amplified and digitized by the Fast Analytical Sensing Technology (FAST) 16mkIII (Quanteon, LLC; Nicholasville, KY) electrochemistry instrument.

mPD Electropolymerization

A minimum of 72 hours after enzyme coating, all Pt recording surfaces were electroplated with 5-mM mPD in 0.05-M phosphate-buffered saline (28). FAST electroplating software applied a potential as a triangular wave with an offset of −0.5 V, peak-to-peak amplitude of 0.25 V, at a frequency of 0.05 Hz, for 20 minutes to create a size exclusion layer that restricts the passage of AA, DA, uric acid, and 3,4-dihydroxyphenylacetic acid.

Calibration

A minimum of 24 hours after mPD electropolymerization, each MEA was calibrated in vitro prior to implantation to generate a standard curve for the conversion of current to glutamate concentration (29). The Pt recording sites and a glass Ag/AgCl reference

electrode (Bioanalytical Systems, West Lafayette, IN) were placed in a continuously stirred solution of 0.05-M phosphate-buffered saline (40.0 mL) maintained at 37°C with a recirculating water bath (Stryker, Kalamazoo, MI). Final beaker concentrations of 250-µM AA, 20-, 40-, and 60-µM l-glutamate, 2-µM DA, and 8.8-µM H_2O_2 were used to assess MEA performance (Figure 1C). Eighteen MEAs (13 unique) were used in the present study. The average ± standard error of the mean (*SEM*) for glutamate sensitivity was 9.7 ± 1.0 pA/µM (R^2 = .995 ± .003), selectivity ratio of 805 ± 327 to 1, and limit of detection of 0.45 ± 0.26 µM based on a signal-to-noise ratio of 3.

MEA/Micropipette assembly

A glass micropipette (1.0-mm outer diameter, 0.58-mm internal diameter; World Precision Instruments, Sarasota, FL) was used to locally apply solutions to the mouse hippocampal subfields. Glass micropipettes were pulled using a vertical micropipette puller (Sutter Instrument, Novato, CA), and the tip was "bumped" to create an internal diameter of 12–15 µm. The tip of the micropipette was positioned between the pair of recording sites and mounted 100 µm above the MEA surface. The micropipettes were filled with sterile filtered (0.20 µm) 70-mM KCl (70-mM KCl, 79-mM NaCl, and 2.5-mM $CaCl_2$, pH 7.4). Fluid was pressure-ejected from the glass micropipette using a Picospritzer III (Parker-Hannafin, Cleveland, OH), with pressure (5–15 psi) adjusted to consistently deliver volumes between 100 and 200 nL over 1- to 2-second intervals. Ejection volumes were monitored with a stereomicroscope (Luxo, Elmsford, NY) fitted with a calibrated reticule (30).

Reference electrode

A Ag/AgCl reference electrode was prepared by stripping 5 mm of Teflon from each end of a silver wire (200 µm bare, 275 µm coated; A-M Systems, Carlsberg, WA). One of the stripped ends was soldered to a gold-plated test connector (Newark element14, Chicago, IL) and the other end was coated with AgCl by placing the tip of the stripped sliver wire (cathode) into a 1-M HCl plating bath saturated with NaCl containing a stainless steel wire (anode) and applying +9 V DC using a power supply to the cathode versus the anode for 15 minutes.

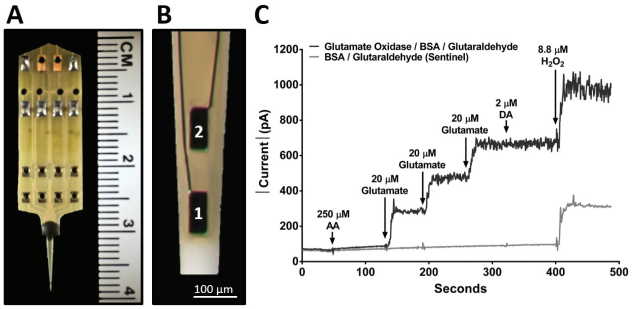

Figure 1. Microelectrode array (MEA) and in vitro calibration. (**A**) Image of the R2 MEA used for anesthetized recordings with a ruler for scale comparison and (**B**) magnified tip depicting 2 Pt recording sites, each measuring 50 × 100 µm with 100-µm spacing between sites. (**C**) A typical MEA in vitro calibration measuring the change in current on a glutamate measuring site (black) and a sentinel recording site (gray) with the addition of multiple analytes, as indicated (↓). The addition of interferents such as l-ascorbic acid (AA) and dopamine hydrochloride (DA) produced no current change on either site because they are blocked by the mPD exclusion layer. Three glutamate additions showed a stepwise increase of current on the glutamate oxidase/bovine serum albumin (BSA)/glutaraldehyde site, but no response on the BSA/glutaraldehyde sentinel site. The addition of H_2O_2 produced a similar increase of current on both recording sites demonstrating equivalent functionality.

In Vivo Anesthetized Recordings

At least 1 week following the MWM probe challenge, mice were anesthetized using 1.5–2.0% isoflurane (Abbott Lab, North Chicago, IL) from a calibrated vaporizer (Parkland Scientific, Coral Springs, FL) and prepared for in vivo electrochemical recordings (22). The mouse was placed in a stereotaxic frame (David Kopf Instruments, Tujunga, CA) fitted with a mouse anesthesia mask, and body temperature was maintained at 37°C with a hydrothermal pad connected to a recirculating water bath. A craniotomy was performed to access the DG (AP: −2.0, ML: ±1.0, DV: −2.2 mm), CA3 (AP: −2.0, ML: ±2.0, DV: −2.2 mm), and CA1 (AP: −2.0, ML: ±1.0, DV: −1.7 mm) from Bregma based on the co-ordinates of Paxinos and Franklin (31). A Ag/AgCl reference wire was implanted in the right cortex, remote from the recording area. The MEA/micropipette assembly was lowered into the DG, CA3, or CA1 (hippocampal subfield and hemisphere randomly assigned for each mouse) using a microdrive (Narishige International, East Meadow, NY) attached to the electrode holder of the stereotaxic arm. Constant potential amperometry (4 Hz) was performed using the FAST16mkIII and FAST software for multichannel simultaneous recordings (32). MEAs were allowed to reach a stable baseline for 60 minutes, at which time basal glutamate measures were taken (10 seconds average) followed by pressure ejection studies. All values for pressure ejections refer to changes versus baseline. After pressure ejection studies, brains were removed and fixed in 4% paraformaldehyde followed by 0.1 M phosphate buffer containing 30% sucrose for at least 24 hours before cryosectioning for immunohistochemistry (45 µm).

Immunohistochemical Staining and Semiquantification

Immunohistochemistry in the hippocampus was performed using rabbit polyclonal GFAP (1:2,000) or guinea pig polyclonal VGLUT1 antibody (1:1,000). Briefly, primary antibodies were applied to serial sections taken for every sixth section from the hippocampus based on our previous protocols (33). Endogenous peroxidase activity was quenched by treating sections with 10% H_2O_2 in 20% methanol for 10 minutes. Sections were then permeabilized in TBST (Tris-buffered saline with 0.25% TritonX-100) following treatment for 20 minutes with sodium metaperiodate. Nonspecific binding was controlled by incubation in 10% normal goat serum for 1 hour. Sections were then incubated overnight in the primary antibody at room temperature. The next day, sections were incubated for 1 hour with the secondary antibody (1:200; biotinylated goat anti-rabbit serum or biotinylated goat anti-guinea pig serum) and 1 hour with the ABC kit. The reaction was developed using the VIP peroxidase substrate kit to enhance the reaction and produce a color stain. This reaction was stopped using 0.1-M phosphate buffer, and the sections were mounted on glass slides, dehydrated, and cover-slipped with DPX. To control for staining intensity, staining of all sections for each antibody was conducted on the same day and developed with VIP for the same amount of time (GFAP: 3 minutes, VGLUT1: 2 minutes).

Staining intensities of GFAP and VGLUT1 in the hippocampus were determined using National Institutes of Health Image J Software 1.48 to measure a gray scale value within the range of 0–256, where 0 represents white and 256 represents black. A template for the DG, CA3, and CA1 subregions of the hippocampus

was created and used on all brains similarly, and images were captured with a Nikon Eclipse E-600 microscope equipped with an Olympus-750 video camera system, and a Dell Pentium III computer. Measurements were performed blinded, and approximately six sections were averaged to obtain one value per subject. Staining density was obtained when background staining was subtracted from mean staining intensities on every sixth section through the hippocampus.

Data Analysis

The FAST16MkIII electrochemical instrument and FAST software save amperometric data, time, and pressure ejection events for all Pt recording sites. Calibration data, in conjunction with a MATLAB (MathWorks, Natick, MA) graphic user interface program developed by Jason Burmeister Consulting, LLC (Version 6.1), were used to calculate basal glutamate and 70-mM KCl-evoked glutamate release and uptake. To determine extracellular glutamate concentration, the sentinel site current (pA) was subtracted from the glutamate recording site current (pA) and divided by the slope (pA/μM) obtained during the calibration (32,34–36). Basal glutamate was calculated by taking a 10-second baseline average prior to start of pressure ejection in the DG, CA3, and CA1. For stimulus-evoked glutamate studies, five reproducible signals were obtained in each hippocampal subfield. These signals were then averaged into a single data point for each hippocampal subfield per mouse for comparison between genotypes. Glutamate uptake followed first-order-rate kinetics; therefore, the uptake rate constant (k_{-1}) was calculated as the logarithmic slope of glutamate concentration versus time (s^{-1}) estimated by use of regression analyses ($R^2 \geq .9$). Because of different cell types and afferent inputs, hippocampal subfields were analyzed independently. Prism software (GraphPad Software, La Jolla, CA) was used for all statistical analyses. A two-way analysis of variance with Tukey's multiple comparison's post hoc test was used to analyze MWM training data. An unpaired, two-tailed Student's *t* test was used to analyze MWM probe, electrochemical, and immunohistochemical data in each hippocampal subfield. Comparisons between MWM and glutamate electrochemical data were established using Pearson correlation. Outliers, determined using Grubbs' test with an alpha of .05, were removed prior to analysis (no more than one per genotype). Data are represented as mean ± *SEM*, and significance was defined as *p* less than .05.

Results

MWM Training and Probe Challenge

Learning and memory were assessed using an 8-day MWM behavioral paradigm as previously described (20). A significant increase by the fifth training day, relative to the first training day, in the path efficiency ($F(4,72) = 13.72$; $p < .0001$) to reach the hidden escape platform was observed for the littermate controls and GHR-KO mice with no differences observed between the two genotypes on any day (Figure 2A), indicating that both genotypes were able to consolidate memories and there were no learning-related genotypic differences. During the probe challenge, littermate controls took a less efficient path (0.16 ± 0.04; $F(9,9) = 2.844$; $p = .0280$) to first platform entry compared with GHR-KO mice (0.37 ± 0.07, respectively), indicating that littermate controls had impaired memory (Figure 2B). Representative probe challenge tracks for littermate controls and GHR-KO mice are shown in Figure 2C and D, respectively.

Basal Glutamate

Prior to stimulus-evoked glutamate release, basal glutamate measures were assessed in each of the hippocampal subfields. Littermate control basal glutamate (Figure 3A) was elevated compared with GHR-KO mice in the DG (2.6 ± 0.5 μM, 0.9 ± 0.3 μM; $F(6,6) = 3.582$; $p = .0099$), CA3 (3.1 ± 0.4 μM, 1.2 ± 0.4 μM; $F(6,6) = 1.232$; $p = .0029$), and CA1 (4.3 ± 0.8 μM, 1.2 ± 0.5 μM; $F(7,6) = 3.134$; $p = .0055$). A negative correlation ($r = -.5619$; $p = .0365$) was observed between CA3 basal glutamate and path efficiency to first platform entry during the MWM probe trial (Figure 3B).

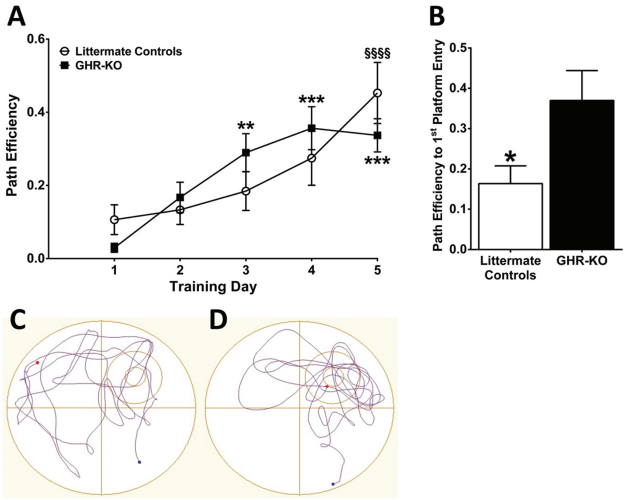

Figure 2. Memory impairment in littermate controls. Morris water maze (MWM) training sessions indicate that path efficiency (**A**) to locate the hidden platform was significantly increased over time for littermate controls and growth hormone receptor knockout (GHR-KO) mice ($n = 10$ per group). By the fifth training session, both genotypes took similar paths to reach the platform indicating comparable learning. Two-way analysis of variance indicates a significant ($p < .001$) effect of training day. $^{**}p < .01$, $^{***}p < .001$ vs GHR-KO training day 1 and $^{§§§§}p < .0001$ vs littermate control training day 1 based on a Tukey's multiple comparison post hoc. MWM probe challenge indicates that littermate controls took a less efficient path (**B**) to first platform entry compared with GHR-KO mice. Two-tailed Student's *t* test ($n = 10$ mice per group), $^{*}p < .05$. Representative MWM probe tracks from (**C**) littermate controls and (**D**) GHR-KO mice. The small circle represents the previous location of the hidden escape platform, whereas the circle surrounding the platform represents the annulus 40.

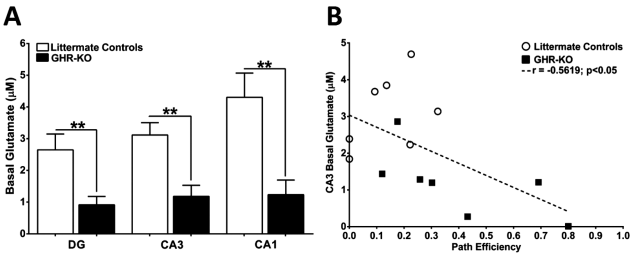

Figure 3. Elevated CA3 basal glutamate predicts Morris water maze (MWM) impairments. (**A**) Bar graphs depicting elevated basal glutamate in all hippocampal subfields of littermate controls compared with growth hormone receptor knockout (GHR-KO) mice. Two-tailed Student's *t* test ($n = 7$–8 mice per group), $^{**}p < .01$. (**B**) Correlation of CA3 basal glutamate with MWM probe path efficiency to first platform entry for littermate controls (open circles) and GHR-KO mice (dark squares). Dashed line represents the least squares regression.

Stimulus-evoked Glutamate Release

We locally applied consistent volumes of 70-mM KCl to littermate controls and GHR-KO mice in the DG (158 ± 7 nL, 147 ± 4 nL; $F(9,7) = 3.555$; $p = .2008$), CA3 (152 ± 5 nL, 155 ± 10 nL; $F(9,7) = 2.447$; $p = .8040$), and CA1 (149 ± 6 nL; 153 ± 5 nL; $F(9,6) = 1.560$; $p = .6239$) to evoke glutamate release (Figure 4A). As shown in Figure 4B, local application of 70-mM KCl elicited robust, reproducible glutamate signals in the CA3 of littermate controls and GHR-KO mice. These glutamate signal patterns were observed in all three hippocampal subfields studied. The average maximal stimulus-evoked glutamate release was significantly elevated in the littermate controls versus GHR-KO mice in the DG (4.9 ± 1.0 µM, 2.3 ± 0.5 µM; $F(9,7) = 3.984$; $p = .0452$), CA3 (9.1 ± 0.9 µM, 3.7 ± 0.5 µM; $F(9,7) = 4.772$; $p = .0002$), and CA1 (3.7 ± 0.6 µM, 2.0 ± 0.2 µM; $F(9,6) = 12.91$; $p = .0332$) as shown in Figure 4C. No statistical differences between stimulus-evoked glutamate uptake were observed between the littermate controls and GHR-KO mice in DG (0.4 ± 0.2 µM/s, 0.7 ± 0.2 µM/s; $F(8,7) = 1.647$; $p = .3392$), CA3 (2.0 ± 0.5 µM/s, 1.1 ± 0.3 µM/s; $F(9,7) = 3.263$; $p = .1470$), or CA1 (0.6 ± 0.2 µM/s, 0.7 ± 0.3 µM/s; $F(8,7) = 2.673$; $p = .4228$) (Figure 4D).

Histological Assessment

Littermate control GFAP (Figure 5A) was decreased compared with GHR-KO mice in the DG (10.6 ± 1.3, 15.3 ± 1.3; $F(8,7) = 1.121$; $p = .0236$), CA3 (12.7 ± 0.5, 15.9 ± 1.0; $F(7,8) = 3.089$; $p = .0096$), and CA1 (8.7 ± 0.6, 12.5 ± 0.8; $F(7,8) = 1.684$; $p = .0016$). Representative images of GFAP staining in whole hippocampus for littermate controls and GHR-KO mice are shown in Figure 5B and C, respectively. Magnified images of the DG, CA3, and CA1 for littermate controls (Figure 5D, F, and H, respectively) and GHR-KO mice (Figure 5E, G, and I, respectively) are presented. We observed hippocampal brain region and genotype-dependent changes in VGLUT1 staining. Littermate controls' VGLUT1 (Figure 6A) was decreased compared with GHR-KO mice in the DG (4.5 ± 0.6, 12.3 ± 0.8; $F(7,8) = 1.633$; $p < .0001$), no change in the CA3 (6.8 ± 0.8, 8.7 ± 1.0; $F(7,8) = 1.163$; $p = .1476$), and increased in the CA1 (8.2 ± 0.9, 5.2 ± 0.5; $F(8,7) = 3.997$; $p = .0133$). Representative images of VGLUT1 staining in the DG, CA3, and CA1 of littermate controls and GHR-KO mice are shown in Figure 6B–G.

Discussion

The glutamatergic system plays an important role in age-related cognitive decline and cognitive disorders, and tight regulation of glutamate is essential for normal brain/cognitive function. Generally, the two major means of controlling both tonic and phasic glutamate neurotransmission are through glutamate release and uptake. Under normal conditions, glutamate release is primarily accomplished through depolarization of glutamatergic neurons, which can be identified by the presence of VGLUTs located at the terminals. Glial cells, composed of astrocytes and microglia, are predominantly responsible for clearance of glutamate from the extracellular space mediated through surface expression of excitatory amino acid transporters (EAATs). One EAAT, Glt-1 (EAAT2 in humans), is responsible for ~90% of glutamate clearance from the extracellular space

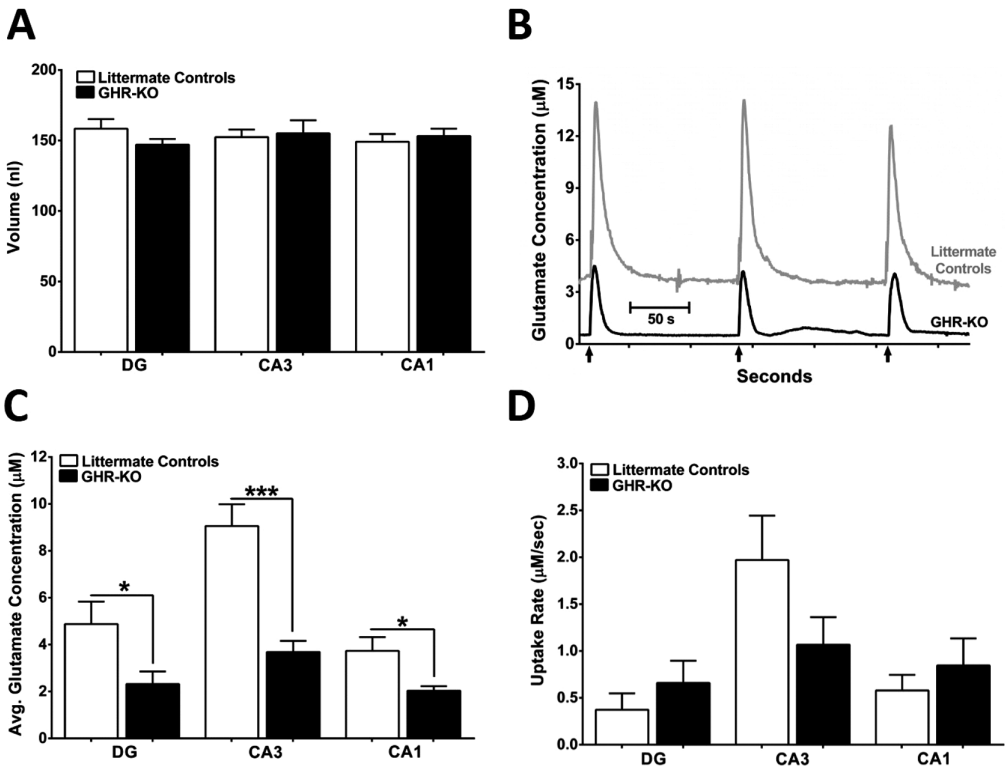

Figure 4. Stimulus-evoked glutamate release and uptake. (**A**) Bar graph depicting a similar range of 70-mM KCl (stimulus) was used to elicit glutamate release in all hippocampal subfields of both mouse genotypes. (**B**) Representative traces of local application (↑) of 70-mM KCl-evoked glutamate release in the CA3 of littermate controls (top, gray) and growth hormone receptor knockout (GHR-KO; bottom, black) mice. (**C**) Bar graphs of average maximal evoked glutamate was elevated in all hippocampal subfields of littermate controls compared with GHR-KO mice. (**D**) Glutamate uptake rate was not significantly different between genotypes in any of the three hippocampal subfields. Two-tailed Student's *t* test (n = 7–10 mice per group), $^*p < .05$, $^{***}p < .001$.

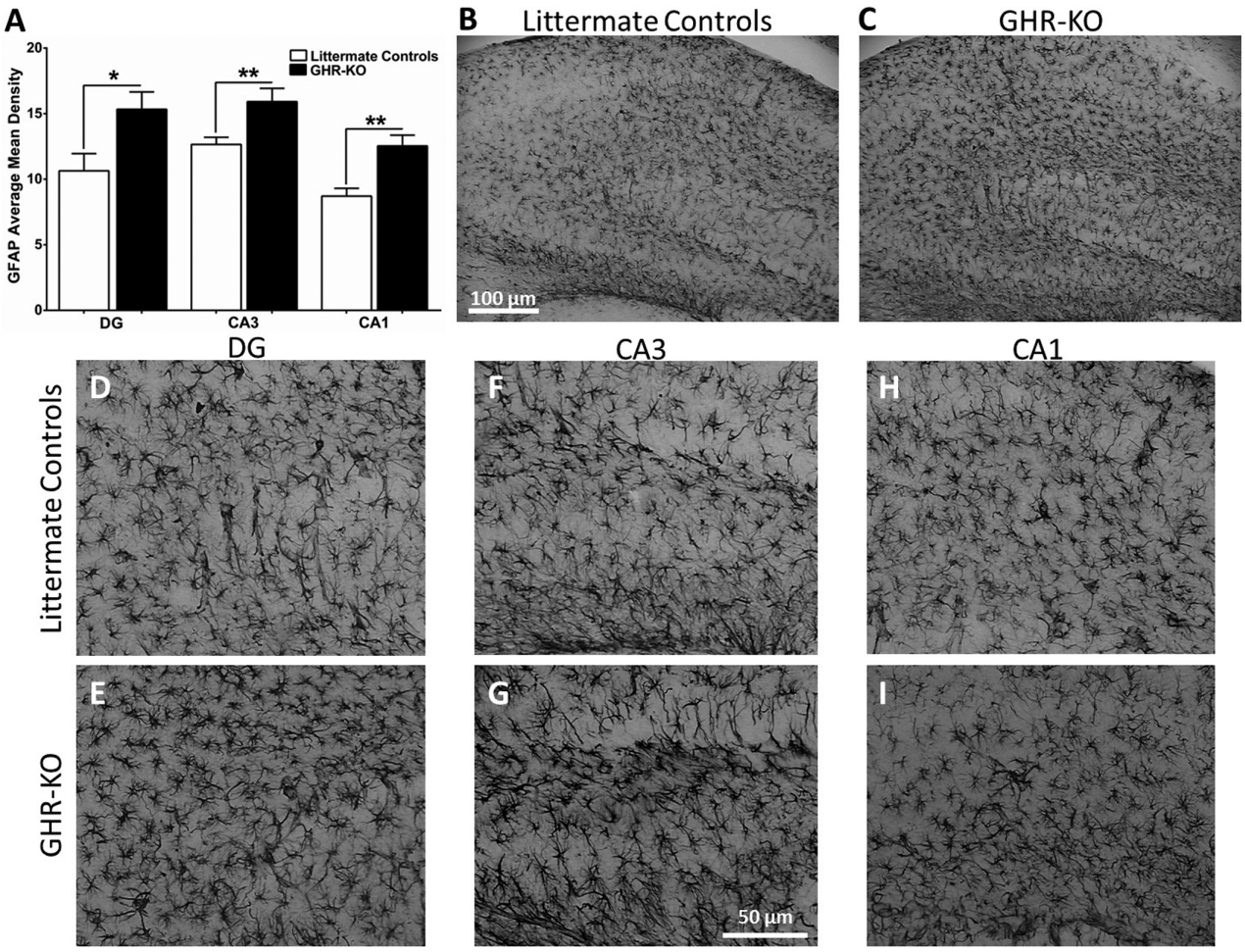

Figure 5. Hippocampal glial fibrillary acidic protein (GFAP) levels. Histological staining of GFAP in the hippocampus of littermate controls and GHR-KO mice. (**A**) Bar graph of GFAP average mean density was elevated in all hippocampal subfields of growth hormone receptor knockout (GHR-KO) mice compared with littermate controls. Two-tailed Student's *t* test ($n = 8$–9 mice per group), $^{*}p < .05$, $^{**}p < .01$. Representative images of GFAP staining in whole hippocampus for (**B**) littermate controls and (**C**) GHR-KO mice (scale bar = 100 µm). Representative magnified images of littermate control and GHR-KO mice DG (D, E, respectively), CA3 (F, G, respectively), and CA1 (H, I, respectively). Scale bar = 50 µm.

(37). Additionally, Glt-1 surface expression and function decrease with age, possibly leading to excitotoxicity, which may be exacerbated in age-related cognitive disorders, further supporting the importance of proper glutamate system maintenance for cognitive retention in advanced age (17). We have previously reported on age-related changes in glutamatergic markers, including elevated mRNA expression of GLT-1 and retained VGLUT1 levels in the hippocampus of long lived GHR-KO mice compared with age-matched littermate controls (12). In the present study, we examine cognition and glutamatergic neurotransmission dynamics to elucidate the role of glutamate in GHR-KO mice that exhibit enhanced cognition in old age compared with age-matched littermate controls.

Our MWM data support that 20- to 24-month-old littermate controls and GHR-KO mice learn to locate the hidden escape platform, indicating no differences in memory consolidation. However, after a 48-hour delay, littermate controls present with impaired memory retrieval compared with GHR-KO mice during the probe challenge of the task. Although it is well known that memory retention declines with age in mice (38,39), previous studies utilizing the inhibitory avoidance, open field, and MWM tasks indicate that memory retrieval in GHR-KO mice does not decline with age (40–42). This may be the result of more stringent regulation of the glutamate system in the hippocampus, as supported by our previous findings (12). Therefore, a possible explanation for improved memory retrieval in GHR-KO mice is that they experience delayed aging thereby postponing the onset of cognitive decline (40).

The dorsal hippocampus is important for consolidation and retrieval of spatial memory during the MWM task (21). Hippocampal inhibition of the EAATs, and therefore decreased glutamate clearance, has been shown to induce long-term depression mediated through elevated extrasynaptic glutamate binding to the GluN2B-NMDA receptor subtype (43) and negatively impacting cognition. In support of this, we observed a negative correlation between CA3 basal glutamate and path efficiency to first platform entry on the MWM task, however, this correlation was not observed with DG or CA1 basal glutamate. This may be due to of the importance of mossy fiber projections to the CA3 subfield for memory consolidation and retrieval in spatial navigation tasks (44,45). Therefore, the increased availability of basal glutamate to activate GluN2B in the CA3 may contribute to the cognitive decline observed in littermate controls while the corollary is true in GHR-KO mice. Furthermore, we observed elevated GFAP staining

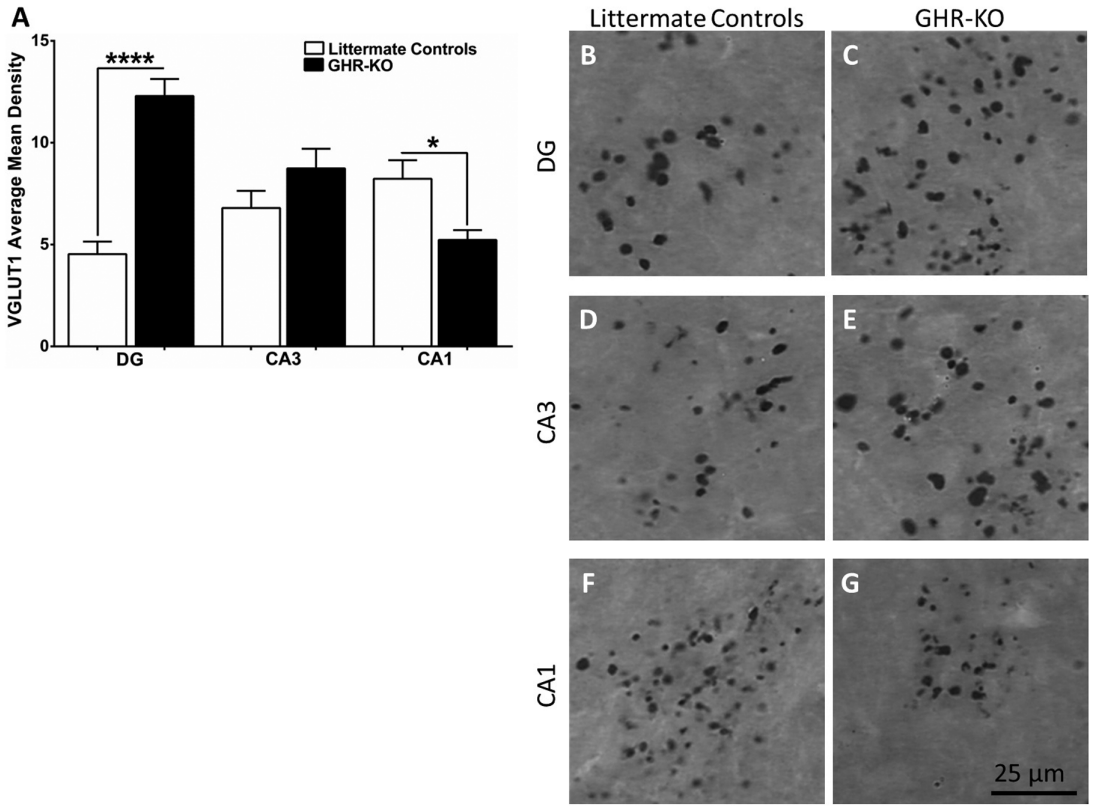

Figure 6. Hippocampal VGLUT1 levels. Histological staining of VGLUT1 in the hippocampus of littermate controls and GHR-KO mice. (**A**) Bar graph of VGLUT1 average mean density in littermate controls was decreased compared with growth hormone receptor knockout (GHR-KO) mice in the DG, no change in the CA3, and increased in the CA1. Two-tailed Student's *t* test (n = 8–9 mice per group), *$p < .05$, ****$p < .0001$. Representative images of littermate control and GHR-KO mice DG (B, C, respectively), CA3 (D, E, respectively), and CA1 (F, G, respectively). Scale bar = 25 µm.

in the hippocampus of GHR-KO mice indicating an increase in glia, which likely contributed to the overall decrease in glutamatergic tone in these mice.

We observed decreased evoked release of glutamate in GHR-KO mice in all three hippocampal subregions examined compared with age-matched littermate controls. This may be explained by previous reports (12) of an age-related decrease in VGLUT1 mRNA levels from whole hippocampus in littermate controls, but not in GHR-KO mice. Further evaluation of 20- to 24-month-old female GHR-KO and littermate control mice presented in this article using histological techniques revealed hippocampal subregion–dependent changes in VGLUT1. However, this is contradictory to our evoked glutamate release data where littermate controls exhibited elevated glutamate release compared with GHR-KO mice. This likely indicates a disconnect between the number of glutamate terminals (VGLUT1) and the inherent excitability of the neurons (stimulated release). It is also possible that the anesthetic used during our glutamate recordings (isoflurane) preferentially suppressed KCl-evoked glutamate release in GHR-KO mice. However, this is highly unlikely because isoflurane dosage was kept consistent (1.5–2.0%) between mice. Furthermore, GHR-KO mice have a higher metabolic rate than littermate controls and therefore would metabolize isoflurane more quickly, if anything, thereby having less anesthetic-related alterations.

Because basal glutamate levels are regulated by a combination of continuous release and uptake, we are not able to directly measure clearance kinetics as we can with stimulus-evoked glutamate release. However, we did not observe any difference in 70-mM KCl-evoked glutamate uptake between genotypes in any of the hippocampal subfields studied despite a significant difference in GFAP levels, possibly because there was sufficient GLT-1 present in close proximity and functioning adequately enough to quickly clear evoked glutamate released from both genotypes. We observed significantly more GFAP in all three hippocampal subregions examined in GHR-KO mice compared with littermate controls. It is possible that the increased energy demands of GHR-KO mice compared with littermate controls (46) may lead to an increase in astrocytes (the main location of glycogen in the brain) to ensure that the brain has sufficient energy, with glutamate uptake into astrocytes contributing to the store of available energy (47,48). Although an increase in GFAP does not always indicate elevated GLT-1, our previous data indicate elevated GLT-1 mRNA in GHR-KO hippocampus (12). Because GLT-1 accounts for 90% of glutamate uptake (37), a decrease in this transporter may slow glutamate clearance, leading to the elevated basal glutamate observed in the littermate controls. However, it should be noted that mRNA levels do not necessarily correspond to protein levels or even surface expression, and it is possible that experimental design limitations may have contributed to this discrepancy between elevated GFAP and GLT-1, but no differences in the uptake rate of evoked release of glutamate. First, EAATs are electrogenic, and membrane depolarization slows glutamate uptake (49). Second, isoflurane, the anesthetic used in this study, increases glutamate uptake through GLT-1 (50). Although, the amount of stimulus and anesthetic were consistent in all mice, it is possible that the combination of these two phenomena could alter

GLT-1 such that their effects overshadow differences in transporter number when measured with our recording technique.

Additionally, glucocorticoids may contribute to elevated basal and stimulus-evoked glutamate release in the littermate control mice. Glucocorticoids have the potential to increase basal glutamate levels in the hippocampus and impair memory through binding of glutamate to the GluN2B-containing NMDA receptor (51), which may also be affected by isoflurane. Although Hauck and colleagues (52) demonstrated that there was no difference in corticosterone levels in 4- to 5-month-old female GHR-KO and littermate control mice under stressed and nonstressed conditions, to date glucocorticoid levels have not been examined in aged female GHR-KO mice. Previous studies support that glucocorticoid levels increase as female mice age contributing to age-related bone loss (53). Considering GHR-KO mice are a model of delayed aging, it goes to reason that glucocorticoid levels may be increased in littermate controls compared with GHR-KO mice, potentially contributing to the elevated extracellular glutamate observed in this study.

In summary, we have demonstrated that littermate controls have impaired cognition and hyperglutamatergic signaling in the DG, CA3, and CA1 hippocampal subfields compared with GHR-KO mice. Cognitive performance on the MWM behavioral task was predicted by CA3, but not by DG or CA1, basal glutamate and elevated GFAP observed in GHR-KO mice may be neuroprotective by contributing to decreased basal glutamate levels. Taken together, these data and our recent reports of elevated evoked glutamate release in the hippocampus of APP/PS1 mice, a model of Alzheimer's disease (20), support an overarching theme whereby elevated hippocampal glutamate is associated with cognitive impairment and maintenance of the glutamatergic system throughout life is essential for the preservation of cognition in aging and age-related neurodegenerative disorders. Furthermore, these data support the importance of glutamatergic regulation for learning and memory in the GHR-KO mouse model of successful aging that may relate to cognitive resilience and could have implications as therapeutic targets to delay the onset of, or reduce cognitive decline, in several diseases and disorders, including Alzheimer's disease.

Funding

This work was supported by the Center for Alzheimer's Disease and Related Disorders at Southern Illinois University School of Medicine, the Kenneth Stark Endowment, the National Institute on Aging at the National Institutes of Health (R01 AG019899 and P01 AG31736), and the state of Ohio's Eminent Scholars Program which includes a gift by Milton and Lawrence Goll to J.J.K.

Conflict of Interest

The authors declare no competing financial interests.

References

1. Ding J, Sackmann-Sala L, Kopchick JJ. Mouse models of growth hormone action and aging: a proteomic perspective. *Proteomics*. 2013;13(3–4):674–685. doi:10.1002/pmic.201200271
2. Kappeler L, De Magalhaes Filho C, Dupont J, et al. Brain IGF-1 receptors control mammalian growth and lifespan through a neuroendocrine mechanism. *PLoS Biol*. 2008;6(10):e254. doi:10.1371/journal.pbio.0060254.
3. Bartke A. Growth hormone and aging: a challenging controversy. *Clin Interv Aging*. 2008;3(4):659–665.
4. Turnley AM, Faux CH, Rietze RL, Coonan JR, Bartlett PF. Suppressor of cytokine signaling 2 regulates neuronal differentiation by inhibiting growth hormone signaling. *Nat Neurosci*. 2002;5(11):1155–1162. doi:10.1038/nn954
5. Ransome MI, Goldshmit Y, Bartlett PF, Waters MJ, Turnley AM. Comparative analysis of CNS populations in knockout mice with altered growth hormone responsiveness. *Eur J Neurosci*. 2004;19(8):2069–2079. doi:10.1111/j.0953-816X.2004.03308.x
6. Bartke A. Healthspan and longevity can be extended by suppression of growth hormone signaling. *Mamm Genome*. 2016. doi:10.1007/s00335-016-9621-3
7. Laron Z, Kopchick JJ, eds. *Laron Syndrome—From Man to Mouse: Lessons from Clinical and Experimental Experience*. Heidelberg, Germany: Springer.
8. List EO, Sackmann-Sala L, Berryman DE, et al. Endocrine parameters and phenotypes of the growth hormone receptor gene disrupted (GHR-/-) mouse. *Endocr Rev*. 2011;32(3):356–386. doi:10.1210/er.2010-0009
9. Sun LY, Bartke A. Tissue-specific GHR knockout mice: Metabolic phenotypes. *Front Endocrinol (Lausanne)*. 2014;5:243. doi:10.3389/fendo.2014.00243
10. Berryman DE, List EO, Palmer AJ, et al. Two-year body composition analyses of long-lived GHR null mice. *J Gerontol A Biol Sci Med Sci*. 2010;65(1):31–40. doi:10.1093/gerona/glp175
11. Wojcik SM, Rhee JS, Herzog E, et al. An essential role for vesicular glutamate transporter 1 (VGLUT1) in postnatal development and control of quantal size. *Proc Natl Acad Sci USA*. 2004;101(18):7158–7163. doi:10.1073/pnas.0401764101
12. Hascup ER, Wang F, Kopchick JJ, Bartke A. Inflammatory and glutamatergic homeostasis are involved in successful aging. *J Gerontol Biol Sci*. 2015. doi:glv010
13. Francis PT. Glutamatergic systems in Alzheimer's disease. *Int J Geriatr Psychiatry*. 2003;18(suppl 1):S15–S21. doi:10.1002/gps.934
14. Mitew S, Kirkcaldie MTK, Dickson TC, Vickers JC. Altered synapses and gliotransmission in Alzheimer's disease and AD model mice. *Neurobiol Aging*. 2013;34(10):2341–2351. doi:10.1016/j.neurobiolaging.2013.04.010
15. Butterfield DA, Pocernich CB. The glutamatergic system and Alzheimer's disease: therapeutic implications. *CNS Drugs*. 2003;17(9):641–652.
16. Kirvell SL, Esiri M, Francis PT. Down-regulation of vesicular glutamate transporters precedes cell loss and pathology in Alzheimer's disease. *J Neurochem*. 2006;98(3):939–950. doi:10.1111/j.1471-4159.2006.03935.x
17. Maragakis NJ, Dykes-Hoberg M, Rothstein JD. Altered expression of the glutamate transporter EAAT2b in neurological disease. *Ann Neurol*. 2004;55(4):469–477. doi:10.1002/ana.20003
18. Morris R. Developments of a water-maze procedure for studying spatial learning in the rat. *J Neurosci Methods*. 1984;11(1):47–60. doi:10.1016/0165-0270(84)90007-4
19. Vorhees CV, Williams MT. Morris water maze: procedures for assessing spatial and related forms of learning and memory. *Nat Protoc*. 2006;1(2):848–858. doi:10.1038/nprot.2006.116
20. Hascup KN, Hascup ER. Altered neurotransmission prior to cognitive decline in AβPP/PS1 Mice, a model of Alzheimer's disease. *J Alzheimers Dis*. 2015;44(3):771–776. doi:10.3233/JAD-142160
21. Cimadevilla JM, Miranda R, López L, Arias JL. Partial unilateral inactivation of the dorsal hippocampus impairs spatial memory in the MWM. *Brain Res Cogn Brain Res*. 2005;25(3):741–746. doi:10.1016/j.cogbrainres.2005.09.001
22. Hascup KN, Hascup ER. Electrochemical techniques for sub-second neurotransmitter detection in live animals. *Comp Med*. 2014;64(4):249–255.
23. Hascup ER, Af Bjerkén S, Hascup KN, et al. Histological studies of the effects of chronic implantation of ceramic-based microelectrode arrays and microdialysis probes in rat prefrontal cortex. *Brain Res*. 2009;1291:12–20. doi:10.1016/j.brainres.2009.06.084
24. Zhou Y, Xu BC, Maheshwari HG, et al. A mammalian model for Laron syndrome produced by targeted disruption of the mouse growth hormone receptor/binding protein gene (the Laron mouse). *Proc Natl Acad Sci USA*. 1997;94(24):13215–13220.

25. Panici JA, Wang F, Bonkowski MS, et al. Is altered expression of hepatic insulin-related genes in growth hormone receptor knockout mice due to GH resistance or a difference in biological life spans? *J Gerontol A Biol Sci Med Sci*. 2009;64(11):1126–1133. doi:10.1093/gerona/glp111
26. Burmeister JJ, Moxon K, Gerhardt GA. Ceramic-based multisite microelectrodes for electrochemical recordings. *Anal Chem*. 2000;72(1):187–192. doi:10.1021/ac9907991
27. Hascup KN, Rutherford EC, Quintero JE, et al. Second-by-second measures of L-glutamate and other neurotransmitters using enzyme-based microelectrode arrays—Electrochemical methods for neuroscience—NCBI bookshelf. In: Borland AC, Michael LM, eds. *Electrochemical Methods for Neuroscience*. Boca Raton, FL: CRC Press; 2006: 407–450.
28. Hinzman JM, Thomas TC, Burmeister JJ, et al. Diffuse brain injury elevates tonic glutamate levels and potassium-evoked glutamate release in discrete brain regions at two days post-injury: an enzyme-based microelectrode array study. *J Neurotrauma*. 2010;27(5):889–899. doi:10.1089/neu.2009.1238
29. Hascup KN, Hascup ER, Littrell OM, et al. Microelectrode array fabrication and optimization for selective neurochemical detection. In: Marinesco S, Dale N, eds. *Microelectrode Biosensors*. 2013 ed. Humana Press; 2013.
30. Friedemann MN, Gerhardt GA. Regional effects of aging on dopaminergic function in the Fischer-344 rat. *Neurobiol Aging*. 13(2):325–332. doi:10.1016/0197-4580(92)90046-Z
31. Paxinos G, Franklin KBJ. *The Mouse Brain in Stereotaxic Coordinates*. 2nd ed. San Diego, CA: Elsevier Science; 2004.
32. Burmeister JJ, Gerhardt GA. Self-referencing ceramic-based multisite microelectrodes for the detection and elimination of interferences from the measurement of L-glutamate and other analytes. *Anal Chem*. 2001;73(5):1037–1042. doi:10.1021/ac0010429
33. Farrand AQ, Gregory RA, Scofield MD, Helke KL, Boger HA. Effects of aging on glutamate neurotransmission in the substantia nigra of Gdnf heterozygous mice. *Neurobiol Aging*. 2015;36(3):1569–1576. doi:10.1016/j.neurobiolaging.2014.11.017
34. Burmeister JJ, Pomerleau F, Palmer M, Day BK, Huettl P, Gerhardt GA. Improved ceramic-based multisite microelectrode for rapid measurements of L-glutamate in the CNS. *J Neurosci Methods*. 2002;119(2):163–171. doi:10.1016/S0165-0270(02)00172-3
35. Hascup KN, Hascup ER, Stephens ML, et al. Resting glutamate levels and rapid glutamate transients in the prefrontal cortex of the Flinders Sensitive Line rat: a genetic rodent model of depression. *Neuropsychopharmacology*. 2011;36(8):1769–1777. doi:10.1038/npp.2011.60
36. Hascup ER, Hascup KN, Stephens M, et al. Rapid microelectrode measurements and the origin and regulation of extracellular glutamate in rat prefrontal cortex. *J Neurochem*. 2010;115(6):1608–1620. doi:10.1111/j.1471-4159.2010.07066.x
37. Holmseth S, Scott HA, Real K, et al. The concentrations and distributions of three C-terminal variants of the GLT1 (EAAT2; slc1a2) glutamate transporter protein in rat brain tissue suggest differential regulation. *Neuroscience*. 2009;162(4):1055–1071. doi:10.1016/j.neuroscience.2009.03.048
38. Fordyce DE, Wehner JM. Effects of aging on spatial learning and hippocampal protein kinase C in mice. *Neurobiol Aging*. 14(4):309–317. doi:10.1016/0197-4580(93)90116-S
39. Kubanis P, Gobbel G, Zornetzer SF. Age-related memory deficits in Swiss mice. *Behav Neural Biol*. 1981;32(2):241–247.
40. Kinney BA, Coschigano KT, Kopchick JJ, Steger RW, Bartke A. Evidence that age-induced decline in memory retention is delayed in growth hormone resistant GH-R-KO (Laron) mice. *Physiol Behav*. 2001;72(5):653–660. doi:10.1016/S0031-9384(01)00423-1
41. Kinney-Forshee BA, Kinney NE, Steger RW, Bartke A. Could a deficiency in growth hormone signaling be beneficial to the aging brain? *Physiol Behav*. 2004;80(5):589–594. doi:10.1016/j.physbeh.2003.10.018
42. Arum O, Boparai RK, Saleh JK, et al. Specific suppression of insulin sensitivity in growth hormone receptor gene-disrupted (GHR-KO) mice attenuates phenotypic features of slow aging. *Aging Cell*. 2014;13(6):981–1000. doi:10.1111/acel.12262
43. Massey PV, Johnson BE, Moult PR, et al. Differential roles of NR2A and NR2B-containing NMDA receptors in cortical long-term potentiation and long-term depression. *J Neurosci*. 2004;24(36):7821–7828. doi:10.1523/JNEUROSCI.1697-04.2004
44. Lee I, Kesner RP. Encoding versus retrieval of spatial memory: double dissociation between the dentate gyrus and the perforant path inputs into CA3 in the dorsal hippocampus. *Hippocampus*. 2004;14(1):66–76. doi:10.1002/hipo.10167
45. Betourne A, Bertholet AM, Labroue E, et al. Involvement of hippocampal CA3 K(ATP) channels in contextual memory. *Neuropharmacology*. 2009;56(3):615–625. doi:10.1016/j.neuropharm.2008.11.001
46. Longo KA, Berryman DE, Kelder B, et al. Daily energy balance in growth hormone receptor/binding protein (GHR -/-) gene-disrupted mice is achieved through an increase in dark-phase energy efficiency. *Growth Horm IGF Res*. 2010;20(1):73–79. doi:10.1016/j.ghir.2009.08.002
47. Brown AM, Ransom BR. Astrocyte glycogen and brain energy metabolism. *Glia*. 2007;55(12):1263–1271. doi:10.1002/glia.20557
48. Prebil M, Jensen J, Zorec R, Kreft M. Astrocytes and energy metabolism. *Arch Physiol Biochem*. 2011;117(2):64–69. doi:10.3109/13813455.2010.539616
49. Takahashi M, Billups B, Rossi D, Sarantis M, Hamann M, Attwell D. The role of glutamate transporters in glutamate homeostasis in the brain. *J Exp Biol*. 1997;200(Pt 2):401–409.
50. Zuo Z. Isoflurane enhances glutamate uptake via glutamate transporters in rat glial cells. *Neuroreport*. 2001;12(5):1077–1080. doi:10.1097/00001756-200104170-00042
51. Sandi C. Glucocorticoids act on glutamatergic pathways to affect memory processes. *Trends Neurosci*. 2011;34(4):165–176. doi:10.1016/j.tins.2011.01.006
52. Hauck SJ, Hunter WS, Danilovich N, Kopchick JJ, Bartke A. Reduced levels of thyroid hormones, insulin, and glucose, and lower body core temperature in the growth hormone receptor/binding protein knockout mouse. *Exp Biol Med*. 2001;226(6):552–558.
53. Weinstein RS, Wan C, Liu Q, et al. Endogenous glucocorticoids decrease skeletal angiogenesis, vascularity, hydration, and strength in aged mice. *Aging Cell*. 2010;9(2):147–161. doi:10.1111/j.1474-9726.2009.00545.x